Optogluram-2: a subtype-selective photoswitchable positive allosteric modulator for metabotropic glutamate receptor 4

Silvia Panarello[a†], Aleix González-Díez [a§], Alice E. Berizzi [b‡§], Fanny Malhaire[b], Roser Borràs-Tudurí [a], Xavier Rovira [a], Laurent Prézeau [b], Jean-Philippe Pin [b], Cyril Goudet [b], Amadeu Llebaria [a]*and Xavier Gómez-Santacana[a,b]*

a MCS, Institute for Advanced Chemistry of Catalonia – CSIC, Barcelona, Spain. b Institut de Génomique Fonctionnelle, Université de Montpellier, UMR 5203 CNRS and U 1191 INSERM, France.

§ share the same contribution

ABSTRACT

Background and Purpose

Metabotropic Glutamate Receptors (mGlu) regulate multiple functions in the nervous systems and are involved in multiple disorders. However, selectively targeting individual mGlu subtypes with spatiotemporal precision is still an unmet need. Photopharmacology can address this concern by means of photoswitchable compounds such as Optogluram, which is a positive allosteric modulator (PAM) of $mGlu_4$ that enables to optically control physiological responses with a high precision. However, Optogluram is not fully selective and finding $mGlu_4$ PAMs with subtype selectivity may be complicated.

Experimental Approach

New photoswitchable analogues of Optogluram were synthesised with the aim of obtaining photoswitchable PAMs selective for $mGlu_4$ receptor and with improved photoisomerization properties. The photopharmacological profiles of these new compounds were assessed using spectroscopy, functional IP and cAMP assays and computational modelling.

Key Results

Optogluram-2 emerged as a new photoswitchable PAM for $mGlu_4$ receptor and offered improved photoswitching properties and was selective for $mGlu_4$. Optogluram-2 had activity as both PAM and allosteric agonist. The π-π stacking of the thiazole ring in the allosteric pocket of $mGlu_6$ is hypothesised to be responsible of the $mGlu_4$ selectivity.

Conclusion and Implications.

The enhanced photoswitching behaviour and improved selectivity of Optogluram-2 makes it an excellent candidate to study the role of $mGlu_4$ with a high spatiotemporal precision that only photopharmacology can offer. Indeed, the use of Optogluram-2 in tissues where $mGlu_4$ can be co-expressed with other mGlu receptors will help to unravel the complexity of mGlu receptors in neural transmission, pinpointing the role of $mGlu_4$ in such systems.

1. INTRODUCTION

G protein-coupled receptors (GPCR) constitute the largest superfamily of cell surface signalling proteins and regulate many physiological processes through binding a wide variety of endogenous ligands (Fredriksson et al., 2003; Schiöth et al., 2008). Currently, GPCRs are the target of approximately 35% of drugs and are involved in multiple diseases including infections, inflammation, neurological diseases, cardiovascular diseases, cancer, and endocrine disorders (Sriram et al., 2018).

The metabotropic glutamate (mGlu) receptors are a family of class C GPCRs comprising eight receptor subtypes subdivided into three different groups: group I, including $mGlu_1$ and $mGlu_5$; group II, including $mGlu_2$ and $mGlu_3$; and group III, including $mGlu_4$, $mGlu_6$, $mGlu_7$ and $mGlu_8$ (Gregory et al., 2021). mGlu receptors are widely distributed throughout the central and peripheral nervous system and are endogenously activated by glutamate, the main excitatory neurotransmitter in the vertebrates. Each mGlu subtype has specific roles that can be modulated with orthosteric agonists or antagonists, which compete for the glutamate binding site in the extracellular domain (orthosteric site). There are also allosteric modulators, which act in an alternative binding site usually located in the transmembrane domain (allosteric site). The binding of molecules to the allosteric site can result in increased, decreased or unaltered receptor responses. This leads to positive, negative or silent allosteric modulators (PAM, NAM or SAM). Allosteric ligands are generally considered better drug

candidates than the orthosteric ligands since they can modulate the receptor activity without interfering with the endogenous ligand binding (Sheffler et al., 2011; Stansley et al., 2019). Additionally, glutamate is the endogenous ligand for a variety of receptor families that are widely distributed in tissues and associated to different physiological effects. Therefore, it is challenging to obtain fully selective ligands targeting glutamate binding sites. In general receptor allosteric pockets are less conserved than orthosteric sites, and particularly in the case of mGlu receptors this is potentially allowing for the development of selective ligands for specific mGlu subtypes (Luessen et al., 2022).

The importance of glutamatergic signalling and the modulatory nature of mGlu receptor makes them promising drug targets for a variety of psychiatric and neurodegenerative CNS disorders. Therefore, knowledge regarding mGlu receptors has improved exponentially over the last years (Witkin et al., 2022). In general, targeting glutamatergic neurotransmission via allosteric fine-tuning of mGlu receptor activities holds great promise for the management of several CNS diseases, with the potential for fewer side effects and a physiological adjustment to glutamate natural release. $mGlu_5$ and $mGlu_2$ are the main targets for drug development, but $mGlu_4$, $mGlu_1$ and $mGlu_3$ are also promising targets. Small molecules for targeting group III receptors, including $mGlu_6$, $mGlu_7$ and $mGlu_8$ receptors, have been undeveloped, although $mGlu_7$ and $mGlu_8$ are emerging as interesting therapeutic targets for the treatment of stress-related diseases or epilepsy (Girard et al., 2019; Gradini et al., 2015; Nickols et al., 2014).

In particular, there is a growing interest in targeting the metabotropic glutamate receptor subtype 4 ($mGlu_4$) as a therapeutic target to treat diseases, such as Parkinson's disease (PD), epilepsy, anxiety, pain and fear processing (Calabrese et al., 2022; Davis et al., 2013; Pereira et al., 2019; Raber et al., 2015). Selective activation of this receptor, via either subtype selective agonists or PAMs, has been shown to significantly reduce or eliminate motor symptoms in preclinical models of PD (Panarese et al., 2019). Moreover, $mGlu_4$ PAMs have been proposed as potential novel therapeutics for the palliative treatment of some forms of epilepsy (Celli et al., 2019; Marino et al., 2005).However, many group III allosteric modulators have failed in pre-clinical or clinical phases as possible drug candidates targeting mGlu receptors, due to adverse effects, lack of efficacy or cross-activity between the different mGlu subtypes (Rascol et al., 2022). These issues may be related to the high degree of structural and sequence homology of the allosteric binding pockets, which makes it very difficult to obtain selective modulators (Lindsley et al., 2016); but also to the widespread expression of mGlu receptors in different areas of the CNS, which also have different roles depending on the cells in which they are expressed. In this last case, drugs acting in a confined location and time would be desirable.

Indeed, photopharmacology may offer a solution, since it uses the spatiotemporal precision of light to switch *on* and *off* the biological activity of target proteins. Photopharmacology makes use of photoswitchable ligands, which are usually derived from existing drugs but include a photoswitch in their molecular scaffold. Thus, the pharmacological properties can be altered upon irradiation with light of different wavelengths (i.e. photoswitching) (Hüll et al., 2018; Szymański et al., 2013). This avant-garde technique has been widely applied for research purposes, and several photochromic ligands have been described in the literature allowing the optical control of a wide variety of GPCRs (Panarello et al., 2022; Ricart-Ortega et al., 2019). Currently, the use of light-regulated ligands has enabled site-, organ-, tissue-, or even subcellular- specific targeting of mGlu receptors in strictly defined time applications (Bossi et al., 2018; Donthamsetti et al., 2021; Gómez-Santacana et al., 2017; Pittolo et al., 2014, 2019; Ricart-Ortega et al., 2020; Rovira et al., 2016; Zussy et al., 2018).

Regarding group III mGlu receptors, to date one photoswitchable PAM has been reported to date. Optogluram (**1**, Figure1A) was originally designed by applying the azologisation approach on VU0415374 (**2**) (Figure1B), which is a positive allosteric modulator of $mGlu_4$ receptor (Engers et al., 2011). The replacement of amide group flanked by aryl groups in VU0415374 (**2**) for a N=N bridge (i.e. azobond) resulted an excellent strategy, since Optogluram (**1**) was the first photoswitchable ligand for the $mGlu_4$ receptor (Pittolo et al., 2014; Zussy et al., 2018). Its azobenzene scaffold (***¡Error! No se encuentra el origen de la referencia.***) allows a rapid isomerization from *trans* to *cis*-configuration upon illumination with violet light (380 nm) and the *trans*-isomer could be quickly recovered from the *cis*-isomer upon green light illumination (500 nm) or by thermal relaxation. *Trans*-Optogluram (i.e. in the dark) showed nanomolar $mGlu_4$ PAM potency, while upon 380-nm illumination its potency was decreased (figure 1A,C) (Zussy et al., 2018). Optogluram (**1**) was found to be selective over group I and II mGlu receptors, but it was a PAM of $mGlu_6$ receptor in the micromolar range and, in lower extent, of $mGlu_8$ receptors, both belonging to group III mGlu receptors, as $mGlu_4$ receptor does (Zussy et al., 2018).

Since $mGlu_4$ and $mGlu_6$ receptor subtypes are mainly expressed in different locations, Optogluram (**1**) was still considered as good candidate for *in vivo* testing in murine model of inflammatory or neuropathic pain. The application of Optogluram (**1**) in the amygdala of living mice produced acute and reversible analgesic peripheral responses, as well as anxiolytic and anti-

depressive effects in mice suffering from persistent inflammatory pain. In contrast, those effects where significantly reduced upon 380-nm illumination of the amygdala and subsequently restored with 500 nm light (Zussy et al., 2018). This allowed a dynamic "*on/off*" control of pain transmission associated with $mGlu_4$ receptors localized in the amygdala (Pereira et al., 2023; Zussy et al., 2018).

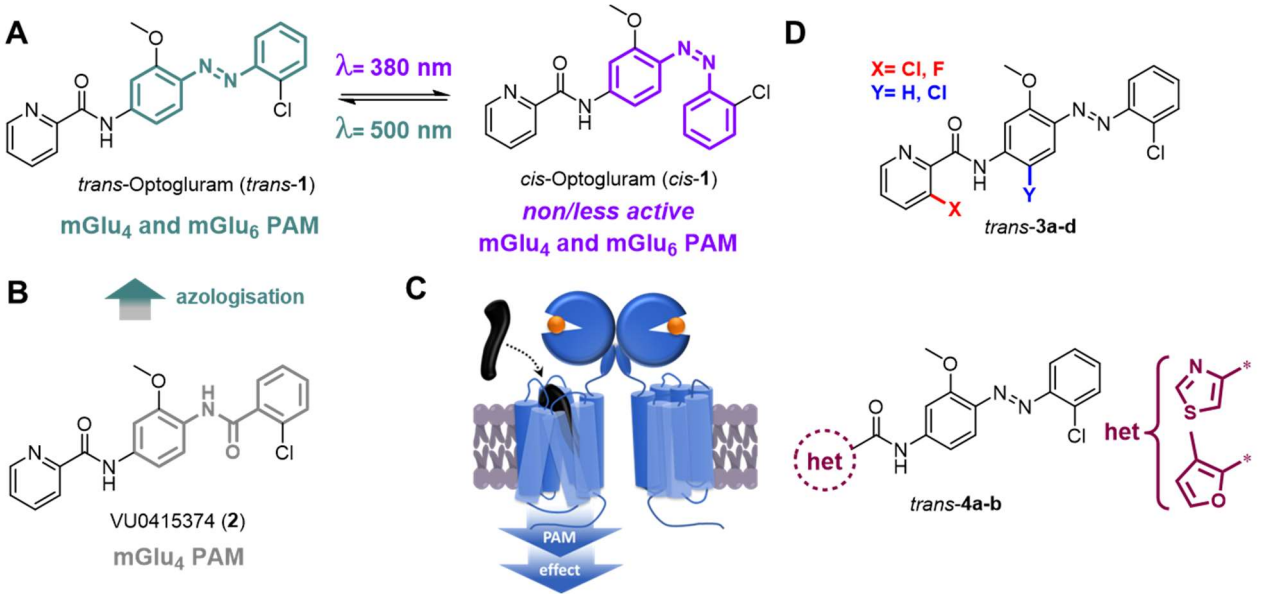

Figure 1: GPCR labelling approaches design. (A) Structure of Optogluram (**1**) as the first photoswitchable allosteric ligand for $mGlu_4$ receptor. Optogluram photoisomerises from *trans* to *cis* configuration or vice versa upon illumination with different wavelengths. (B) Optogluram resulted from an azologisation strategy applied to VU0415374 (**2**), a reported $mGlu_4$ PAM (C). Both trans-Optogluram and VU0415374 bind in the allosteric pocket of $mGlu_4$ receptor. (D) Optimization plan for $mGlu_4$ PAM Optogluram (**1**) to decrease potency at $mGlu_{6/8}$ receptors via analogues **3a-d** and **4a-b**.

In the field of photopharmacology, several photoswitchable allosteric modulators for metabotropic glutamate receptors have been developed. However, there is still considerable work to complete the photopharmacological toolbox (Gómez-Santacana et al., 2022). Indeed, obtaining mGlu allosteric modulators selective among the other subtypes might be a burden, specially within the group III. In this context, we decided to modify the structure of Optogluram (**1**) to generate a small library of azobenzene candidates with the aim of maintaining or enhancing PAM activity on $mGlu_4$ receptor and decreasing that one over the other group III glutamate receptors. Additionally, we deciphered the pharmacological characteristics of those compounds, including a computational analysis of the possible binding mode of the allosteric molecules.

2. METHODS

Organic Synthesis materials and methods

All the chemicals and solvents were provided from commercial suppliers and used without purification, except the anhydrous solvents, which were treated previously through a system of solvent purification (*PureSolv*), degasified with inert gases and dried over alumina or molecular sieves (DMF). All the reactions described below were monitored by thin layer chromatography (60F, 0.2 mm, *Macherey-Nagel*) by visualization under 254 and/or 365 nm lamp. The synthesis of Optogluram analogues **3a-d** and **4a-b** is detailed in the supporting information

Flash column chromatography was performed using silica gel 60 (*Panreac*, 40-63 µm mesh) or by means of SNAP KP-Sil 50 µm (*Biotage*) and/or SNAP KP-C18-HS 50 µm (*Biotage*) columns, automated with Isolera One with UV-Vis detection (*Biotage*).

Nuclear magnetic resonance (NMR) spectra were recorded on a 400 MHz Variant Mercury (*Agilent Technologies*) and on a 400 MHz Brüker Avance NEO instrument. Data were processed using *Mestre Nova V. 8.1* software (*Mestrelab Research*). ^{1}H and ^{13}C chemical shifts are reported in parts per million (ppm) against the reference compound using the signal of the residual non-deuterated solvent [Chloroform ($CDCl_3$) δ= 7.26, 1.56 ppm (^{1}H), δ= 77.16 ppm (^{13}C)]. The following abbreviations have been used to designate multiplicities: s, singlet; d, doublet; t, triplet; m, multiplet; br, broad signal; dd, doublet of doublet; dt, doublet of triplet; ddd, doublet of doublet of doublet. Coupling constants (J) are reported in Hertz (Hz).

Purity determination and absorption UV-Vis spectra were determined with High-Performance Liquid Chromatography Thermo Ultimate 3000SD (*Thermo Scientific Dionex*) coupled to a PDA detector and an LTQ XL ESI-ion trap mass spectrometer (*Thermo Scientific*) or with a Waters 2795 Alliance coupled to a DAD detector (*Agilent 1100*) and an ESI Quattro Micro MS detector (*Waters*). Data from mass and UV-Vis spectra were analysed using *Xcalibur* 2.2 SP1 software (Thermo) or *MassLynx* 4.1 software (Waters) HPLC columns used were ZORBAX Eclipse Plus C18 (4.6 × 150 mm; 3.5 µm) and ZORBAX Extend-C18 (2.1 × 50 mm, 3.5 µm). HPLC purity was determined using the following binary solvent system as general method: 0.05% formic acid in 5% MeCN and 0.05% formic acid in 95% water for 0.5 min, from 5 to 100% MeCN in 5 min, 100% MeCN for 1.5 min, from 100 to 5% MeCN in 2 min and 5% MeCN for 2 min. The flow rate was 0.5 ml/ min, the column temperature was fixed to 35 °C, and wavelengths from 210 to 600 nm were registered. Compound purities were calculated as the percentage peak area of the analysed compound by UV detection at 254 nm. The isomeric ratio of photoswitchable compounds is given considering the % of absorbance at the isosbestic point of the two species.

All high-resolution mass spectra (HRMS) and elemental compositions were performed on a FIA (flux injected analysis) with ultrahigh-performance liquid chromatography (UPLC) *Aquity (Waters)* coupled to LCT Premier Orthogonal Accelerated Time of Flight Mass Spectrometer (TOF) (*Waters*). The following binary solvent system is used: from 10% MeCN in 20 mM formic acid to 100% MeCN in 5 min. Data from mass spectra was analysed by electrospray ionization in positive and negative modes using *MassLynx* 4.1 software (Waters). Given calculated masses are calculated with Chemdraw 20.0. Spectra were scanned between 50 and 1500 Da with values every 0.2 s and peaks are reported as m/z.

Illumination sources. Two different LED illumination systems were used as light sources: Teleopto and CoolLED. The *Teleopto light system* consists of single or dual wavelength LED Array (model LEDA-X and LEDA2-By respectively) connected to a LED Array Driver (model LAD-1). By the mode switch of LAD-1 LED Array Driver is it possible to choose constant or trigger mode, the latter by means a stimulator (STO mkII, version 1.6) which enables time-controlled pulsed stimulation. The light was delivered from the bottom to the solutions since the LED Array perfectly fits for 96 well-plates and each LED element comes just under each well. Teleopto system set at 12 V intensity and in continuous mode corresponds to 0.09 mW/mm^2 for 365 nm, 0.09 mW/mm2 for 380 nm, 0.19 mW/mm^2 for 405 nm, 0.13 mW/mm^2 for 420 nm, 0.17 mW/mm^2 for 455 nm, 0.14 mm2 for 470 nm, 0.10 mW/mm^2 for 500 nm, 0.09 mW/mm^2 for 530 nm and 0.14 mW/mm^2 for 550 nm wavelength. The *CoolLED light system* consists of a liquid light guide accessory (pE-1906, CoolLed) connected to a LED light source (pE-4000, CoolLed). For the photochemical characterization of the samples, the liquid light guide accessory was pointed directly toward each sample placed in transparent 96-well plates so that the light was delivered from the top to the solutions and for three minutes in continuous mode. CoolLED set at 50% intensity corresponds to 1.04 mW/mm2 for 365 nm, 2.60 mW/mm^2 for 385 nm, 2.10 mW/mm^2 for 405 nm, 0.72 mW/mm^2 for 435 nm, 2.17 mW/mm2 for 460nm, 1.02 mW/mm^2 for 470 nm, 0.95 mW/mm^2 for 490 nm, 0.3 mW/mm^2 for 500 nm, 0.36 mW/mm^2 for 525 nm, and 1.57 mW/mm^2 for 550 nm light. Potencies were measured using a Thorlabs PM100D power energy meter connected with a standard photodiode power sensor (S120VC).

UV-Vis spectroscopy. The absorption spectra of the photoisomerisable compounds were obtained with solutions 10-50 µM in DMSO, MeCN, water or in a buffer (PBS or a determined pH buffer) with 0.5-10% DMSO (200 µL of compound solution/well) using a Tecan's Spark 20M Multimode Microplate reader. The samples were measured between 800 and 300 nm with an average time of 50 ms at 2 nm fixed intervals to achieve the full absorption spectra. To evaluate the photoisomerization of the samples and obtain the optimal illumination wavelengths to photoisomerise from *trans* to *cis* configuration by UV-Vis, a continuous illumination for a minimum of three minutes was applied with the corresponding light source mentioned above, on the sample solutions placed in black clear-bottom (Greiner Bio-one) or transparent (Greiner CELLSTAR®) 96-well plates (200 µL of compound solution/well). Immediately after the illumination, the samples were read as indicated above with Tecan's Spark 20M Multimode Microplate reader. The effect of repeated light cycles to sample of 10-50 µM of the compounds in DMSO and PBS, HEPES buffer solution or water was evaluated in order to assess the stability of the photoisomerization. Therefore, multiple *trans*/*cis* isomerization cycles were registered by measuring absorbance at a determined single wavelength with Tecan's Spark 20M Multimode Microplate reader in the dark and after three minutes of constant illumination with the optimal isomerization wavelengths.

Photoisomerization analysis by LC-PDA-MS. The *cis/trans* isomer ratio from photoisomerization of Optogluram-2 (**4a**) was determined by liquid chromatography coupled to a photodiode array and a mass spectrometer detector (LC-PDA-MS). Through the analysis of LC-PDA-MS spectra we quantified the amount of *trans* and *cis* isomers in the dark and upon illumination once reached the photostationary state. The separated peaks were integrated using the PDA channel at the wavelength of the isosbestic point which was previously determined by UV-Vis spectroscopy for each pair of isomers.

Illuminations were performed with *CoolLED light system* in microcentrifuge tube containing 150 µL of 1 mM DMSO solution of each compound for 3 min. Then, 10 µl of the stock solution were taken each time and diluted with 90 µl of MeCN in Amber Glass 9 mm Screw Neck Vial to obtain the final 100 µM sample to be analysed by LC-PDA-MS.

Materials for pharmacological characterisation. HEK 293 cells were obtained from ATCC® CRL-1573™ (Molsheim, France). Human and rat mGlu constructs were prepared in-house. Dulbecco's modified Eagle medium (DMEM), glutamate-free DMEM GlutaMAX, enzyme-free cell dissociation buffer and foetal bovine serum were purchased from Merck-Aldrich. Antibiotics and Polyethylenimine (PEI) were purchased from Merck-Aldrich. The IP_1 assay and cAMP assay kits were provided from REVVITY (Codolet, France).

Cell culture and transient transfections for pharmacological characterisation. The HEK293 (ATCC, CRL-1573) cells were cultured in Dulbecco's modified Eagle's medium (*Gibco* DMEM; *Thermo Fisher Scientific*) supplemented with 10% foetal bovine serum (FBS, *Merck-Aldrich*) and maintained at 37°C in a humidified atmosphere with 5% CO_2. Then the cells were transfected with human mGlu receptor by electroporation or lipofectamine transfection following the manufacturer's protocol (*Invitrogen* Lipofectamine 2000, *Thermo Fisher Scientific)*. For those mGlu receptors that are not naturally linked to the phospholipase C (PLC) signalling pathway ($mGlu_{4,6,8}$), a chimeric $G_{q/i}$-protein (G_q top) was transfected in order to couple receptor activation to the PLC pathway and obtain IP production. We also co-transfected the Excitatory Amino Acid Transporter 3 (EAAC1) to remove the glutamate from the extracellular space, and therefore keep its levels low. The mGlu receptor constructs contained a Flag and SNAP tag to enable the measurement of cell surface receptor expression. Once transfected as previously described (Gómez-Santacana et al., 2017; Ricart-Ortega et al., 2020) the cells were seeded in black clear-bottom 96-well plates at a concentration of $1x10^6$ cells/well. At least 2 h before the experiment, the medium was changed to preheated DMEM Glutamax (*Gibco*, *Thermo Fisher Scientific*), which does not include L-glutamine but contains Glutamax™ supplement.

Generation of HEK 293 stable rat $mGlu_4$ inducible cell line. The stably expressing, inducible rat (r)$mGlu_4$ HEK293 cell line was generated with the Flp-In-T-Rex system according to manufacturer recommendations (*Invitrogen*). The cDNA encoding the $rmGlu_4$ also contained a Flag and SNAP tag in the N terminus (for detection) and the construct was inserted into the pcDNA5-FRT-TO-GFP plasmid (*Addgene*), where it replaced the GFP. This construct was co-transfected with the recombinase plasmid pOG44 (*Invitrogen*), by electroporation, to allow for targeted integration of the expression vector into the same locus of the Flp-In-T-Rex HEK 293 cells (*Invitrogen*), thereby ensuring homogeneous levels of gene expression. Cells were grown for 48 h, before selection was initiated via the addition of 15 µg/mL blasticidin and 100 µg/mL of hygromycine B. Following induction with 1 µg/mL doxycycline (*Sigma-Aldrich*), inducible expression of the $rmGlu_4$ receptor on cells was confirmed by an anti-Flag ELISA assay.

TR-FRET Inositol phosphate (IP) accumulation assay. The *IP-One HTRF Gq* kit assay (REVVITY) was used for the direct quantitative measurement of *myo*-inositol 1-phosphate in HEK293 cells transiently transfected with the human and rat mGlu receptors according to the transfection methodology described above. Cells were stimulated to induce IP accumulation with various concentrations of orthosteric and/or allosteric compounds, depending on the type of the assay, in HTRF stimulation buffer (REVVITY) for 30 min, at 37°C and 5% CO_2 in both dark and under illumination conditions. For the experiments with illumination to induce photoswitching, the *Teleopto light system* was used. Thus, black transparent-bottom 96-well plates (*Greiner Bio-one*) containing the cultured cells were placed over a single or dual wavelength LED Array (model LEDA-X and LEDA2-By respectively) connected to a LED Array Driver (model LAD-1). The light was delivered from the bottom to the solutions since the LED Array perfectly fits for 96 well-plates and each LED element comes just under each well. Light pulses of 50/50 ms (pulse width/interval) was chosen over continuous illumination to reduce cell overheating (especially for wavelengths with higher energy such as 380 nm) and avoid a loss of robustness of the assay. To avoid effects derived from the fast relaxation of photoisomerisable compounds in aqueous solution after the 30-min stimulation and possible interference with the fluorescence reading, the solutions of every well were removed and fresh stimulation buffer was added prior to the lysis step of the assay protocol. TR-FRET fluorescence readings were obtained with PHERAstar FS multimode microplate reader (*BMG-Labtech*) with a delay time of 150 µs between donor excitation and fluorescence readings, as HTRF ratio (665/620). To determine allosteric inactivation, we measured the response of the receptors to high agonist concentrations in both the presence and absence of a competitive antagonist (values used for normalization). Low, high and saturating concentrations of agonists were the same as reported previously (Zussy et al., 2018)..

TR-FRET Cyclic adenosine monophosphate (cAMP) accumulation assay. The *cAMP HTRF Gi* kit assay (REVVITY) was used for the direct quantitative measurement of cyclic adenosine monophosphate (cAMP) in HEK293 cells stably expressing the rmGlu$_4$ receptor according to the expression induction protocol described above. Cells were stimulated to induce cAMP accumulation with various concentrations of orthosteric and/or allosteric compounds in HTRF stimulation buffer (serum-free DMEM Glutamax™ supplemented with IBMX 500 µM) for 30 min at 37°C and 5% CO_2 in both dark and light conditions. For these experiments, we followed a very similar method to that used with *IP-One HTRF Gq* kit assay (REVVITY), previously described. Indeed, the only notable difference in the protocol was the addition of Forskolin 0.75 µM in the cells for the last 15 minutes of incubation in dark and upon illumination. After the lysis, the plate was incubated a minimum 1 hour at room temperature and TR-FRET fluorescence readings were obtained with PHERAstar FS multimode microplate reader (*BMG-Labtech*) with a delay time of 150 µs between donor excitation and fluorescence readings, as HTRF ratio (665/620).

Allosteric interactions. For functional interaction studies between the orthosteric agonist, L-AP$_4$, and allosteric modulators in the cAMP assay, the following operational model of allosterism was applied (Leach et al., 2007).

$$Y = Basal + \frac{(E_M - Basal) \times ((([A](K_B + \alpha\beta[B])) + \tau_B[B] \times EC_{50})^n}{((([A](K_B + \alpha\beta[B])) + \tau_B[B] \times EC_{50})^n + ({EC_{50}}^n \times (K_B[B])^n)}$$

Equation 1

where Basal is the response in the absence of ligand, E_M is the maximum response of the system, EC_{50} is the midpoint of the concentration-response curve of the agonist, [A] and [B] represent the concentrations of the orthosteric agonist, L-AP4, and the indicated allosteric ligand, respectively, and *n* represents the slope of the transducer function that links receptor occupancy to response. K_B is the equilibrium dissociation constant of the allosteric ligand, K_B denotes the capacity of the allosteric ligand to exhibit agonism, and αβ represents the combined affinity/efficacy cooperativity parameter describing the effect of the allosteric modulator on agonist function. The derived cooperativity estimates that are greater than 1 indicate positive cooperativity, while values less than 1 but greater than 0 indicate negative cooperativity and values equal to unity denote neutral cooperativity.

Cell Culture and transfection for real time pharmacological assays. HEK293-H188-M1 (HEK293 cells stably expressing the Epac-S^{H188} cAMP biosensor) were maintained at 37 °C, 5% CO_2 in Dulbecco's modified Eagle medium (DMEM, GIBCO, cat #41965039) supplied with 10% heat-inactivated foetal bovine serum (FBS; GIBCO, cat #11550356).[#1] Cells were grown in T-75 flasks or 10-cm dishes, split when reaching 85−90% confluence and detached by trypsin−ethylenediaminetetraacetic acid (EDTA; Sigma-Aldrich, cat #T3924) digestion. The day before transfection, around 6.0 × 10^6 HEK298-H188-M1 cells were seeded in a 10-cm dish. The following day, the 10-cm dish, with a confluency between 65-75%, was taken and the old medium was removed by aspiration, right after 6 mL of DMEM were added. The transfecting agent employed was polyethyleneimine 1 mg/mL solution (PEI; Polysciences, cat#23966) and the PEI/DNA complexes were prepared as follows: Two sterile 1.5 mL tubes were filled with 500 µL PBS (GIBCO, cat #11550356) each. Then, 10 µg plasmid DNA were added (hmGlu$_4$/EAAC1 2:1) to one of them and to the other tube 30 µL PEI solution were added. At this point, both tubes were vortexed at full speed (3000 rpm) for 1 min and let stand afterwards at room temperature for 10 min. After that, the DNA solution was transferred to the PEI solution, the resulting solution was mixed gently by pipetting up and down three times and it was incubated at room temperature for 3 min. When the time was up, the 1 mL PEI/DNA complexes solution was added dropwise to the 10-cm dish and left in the incubator for 4-5 h (37 °C and 5% CO_2). When the time passed, the old medium containing PEI/DNA complexes was removed and 10 mL of fresh DMEM were added and left in the incubator (37 °C and 5% CO_2) overnight.

General Methods Real-Time pharmacological photoswitching assays*.* The assays were carried out using transiently transfected HEK293-H188-M1 cells transiently expressing hmGlu$_4$ receptor and the excitatory amino acid transporter 1, EAAC1. All assays were performed at room temperature and 48 h after the transfection. The day after the transfection, cells were detached by rinsing once with PBS, followed by incubation with trypsin−EDTA for 5 min until detachment of cells was observed. The detached cells were resuspended with DMEM and 10 µL of the resulting suspension were counted using Neubauer Chamber while the cells were being centrifugated at 1300 rpm for 3 min. The supernatant was carefully removed, and cells were resuspended in DMEM complete medium to obtain a cell solution with 1.0 × 10^6 cells/mL. The cell solution was used to seed 125 000 cells per well in a poly-ornithine coated (Poly-L-ornithine hydrobromide, cat#P3655) transparent 96-well microplate (Thermo Scientific Nunc Microwell, cat#10212811) and left at 37 °C with 5% CO2 for approximately 24h. The cAMP EPAC sensor buffer (14 mM NaCl, 50 nM KCl, 10 nM $MgCl_2$, 10 nM $CaCl_2$, 1 mM *N*-(2-hydroxyethyl)piperazine-*N'*-ethanesulfonic acid (HEPES), 1.82 mg/mL glucose, pH 7.2) was used as the assay medium in FRET-based experiments.

Fluorescence values were measured using a Tecan Spark M20 multimode microplate reader equipped with the Fluorescence Top Standard Module with defined wavelength settings (excitation filter 430/20 nm and emission filters 485/20 and 535/25 nm). The FRET ratio was calculated as the ratio of the donor emission (td^{cp173V}, 485 nm) to the acceptor emission (mTurq2Δ, 535 nm). The FRET ratio was normalized to the effect of the buffer containing the EC_{20} of the agonist (0%) and the response obtained with VU0415374 at the working concentration (100%). External light was applied using the 96-well LED array plate (LEDA Teleopto). Each set of experiments was performed four times with each concentration in triplicate.

Real-Time pharmacological photoswitching assays. After 48 h the transfection, the medium from the 96-well microplate was removed by inversion and then 100 µL per well of glutamate-free DMEM GlutaMAX (GIBCO, cat#31966021) were added 2 h before starting the assay. Afterwards, the DMEM GlutaMAX was removed by inversion and then 80 µL per well of the cAMP EPAC sensor buffer containing 100 µM of 3-Isobutyl-1-methylxanthine (IBMX; Sigma-Aldrich, cat#I5879) were added and it was left at room temperature for 10 min. Meanwhile, a 10x pre-plate containing the final constant concentration of 10 µM VU0415374 and Optogluram-2, 3 µM of VU0415374 and Optogluram was prepared using the cAMP EPAC buffer containing IBMX with a EC_{20} of L-AP4 (30 nM). Then, 10 µL per well of the cAMP EPAC sensor buffer containing forskolin (final concentration 1 µM) was added and left at room temperature for 15 min. Finally, the compounds and IBMX buffer containing EC_{20} of L-AP4 were added and incubated for 1 h at room temperature. After this time the fluorescence was measured. Then, the plate was continuously illuminated with light at 380 nm for 10 min and fluorescence values were recorded. Immediately after, the plate was illuminated in continuous mode for 10 min with light at 455 nm and fluorescence was measured.

Data analysis. All experiments were analysed using GraphPad Prism 8.1.1 (GraphPad Software, San Diego, CA). The HTRF ratios were transformed to the IP or cAMP concentration produced by the cell with a standard IP or cAMP curve. Then, we normalized the top and the bottom values between 0 and 100% of receptor activation with respect to a control compound pharmacologically well-characterised. The fluorescence obtain in the real time photoswitching assays was normalised by the 0 and 100% of receptor activation with respect to the control VU0415374. Data were analysed by two-way ANOVA with time as repeated measure and including the Tukey correction for multiple testing, $*p < 0.05$.

Preparation of cryoEM structure $mGlu_4$ receptor (PDB 7E9H) and docking. The software used was Schrödinger Release 2022-2: Maestro, Schrödinger, LLC, New York, NY, 2022. The prepared chain R from the cryoEM structure 7E9H was employed. The rotameric state of amino acid F801 was manually modified towards the membrane. The known binder used for protein refinement was VU0415374 together with Glide docking with extra precision (Glide-XP). The grid used for the Glide docking was prepared via Receptor Grid Generation protocol followed by the selection of the following amino acids: C636, M663, Y667, L756, L757, W798, S825, S829, S833. The binding pocket was refined by means of Induced-Fit Docking (IFD) using VU0415374 and the aforementioned amino acids to confine the binding pocket. IFD protocol consisted on an initial Glide Docking (the receptor and ligand Van der Waals scaling set to 0.50, and the maximum number of poses to 20) followed by a refinement of residues within 5 Å of ligand poses by Prime and finally a Glide redocking with extra precision. The resulting model from best pose (by both Glide Scoring and visual inspection) was taken as model for the docking of the analogues which was achieved by ligand docking using Glide-XP.

$mGlu_6$ homology modelling based on $mGlu_4$ cryoEM structure and docking. The software used was Schrödinger Release 2022-2: Maestro, Schrödinger, LLC, New York, NY, 2022. The cryoEM structure 7E9H was obtained from Protein Data Bank. The protomer "Chain R" was selected and then the G protein was extracted. Then the prepared chain R and the sequence $mGlu_6$ (extracted from https://www.uniprot.org/, code: O15303) were used as input for the homology modelling tool in Maestro. The parameters were left by default and the generated model was subjected to the Protein Reliability script and, afterwards, to the Protein Preparation Workflow module. All the ligands used were previously duly prepared using LigPrep (Force field OPLS4, retaining specific chirality). The rotameric state of amino acid F799 was manually modified towards the membrane. The grid used for the Glide docking was prepared via Receptor Grid Generation protocol followed by the selection of the following amino acids: I631, T661, Y665, C754, L755, F799, S823, S827, S831. The binding pocket was refined by means of Induced-Fit Docking (IFD) using VU0415374 and the aforementioned amino acids to confine the binding pocket. IFD protocol consisted on an initial Glide Docking (the receptor and ligand Van der Waals scaling set to 0.50, and the maximum number of poses to 20) followed by a refinement of residues within 5 Å of ligand poses by Prime and finally a Glide redocking with extra precision. The resulting model from best pose (by both Glide Scoring and visual inspection) was taken as model for the docking of the analogues which was achieved by ligand docking using Glide-XP.

3. RESULTS

Design of photoisomerisable azocompounds. We designed the new photoswitchable compounds based on Optogluram (**1**), the first photoswitchable positive allosteric modulator (PAM) targeting $mGlu_4$ receptor, discovered in our research group (Pittolo et al., 2014; Zussy et al., 2018). During the optimization process, we decide to preserve the outer 2-chlorophenyl ring and the 3-methoxy substituent in the central aromatic ring since both groups were found important in a series as of $mGlu_4$ PAMs (*e.g.* VU0415374 (**2**), Figure1B), previously reported (Engers et al., 2011). Indeed, other substitutions in these aromatic rings led to a significant decrease in $mGlu_4$ activity. Thus, we decided to focus our structure-activity relationship on key substituents on the picolinamide moiety and the central phenyl ring of Optogluram (**1**). We also replaced the 2-picolyl group by two different five-membered heteroaryl rings. These modifications provided analogues **3a-d** and **4a-b** (Figure1D) . Overall, Optogluram structural modifications were designed to enhance $mGlu_4$ PAM activity over activities at $mGlu_{6/8}$ receptors.

Synthesis Optogluram analogues 3a-d and 4a-b. Optogluram analogues **3a-d** and **4a-b** were prepared following an optimized two-step synthetic route (Scheme 1), in contrast to the 5-step original route used to synthesize Optogluram (**1**). The sequence started with the direct diazotization of 2-chloroaniline (5) followed by the azo-coupling with 3-methoxyaniline (**6a**) or 2-chloro-5-methoxyaniline (**6b**) to yield amino azobenzenes **7a** and **7b**. These amines were acylated with the corresponding carboxylic acids **8a-b**,**9** and **10** to give azo compounds **3a-d** and **4a-b**.

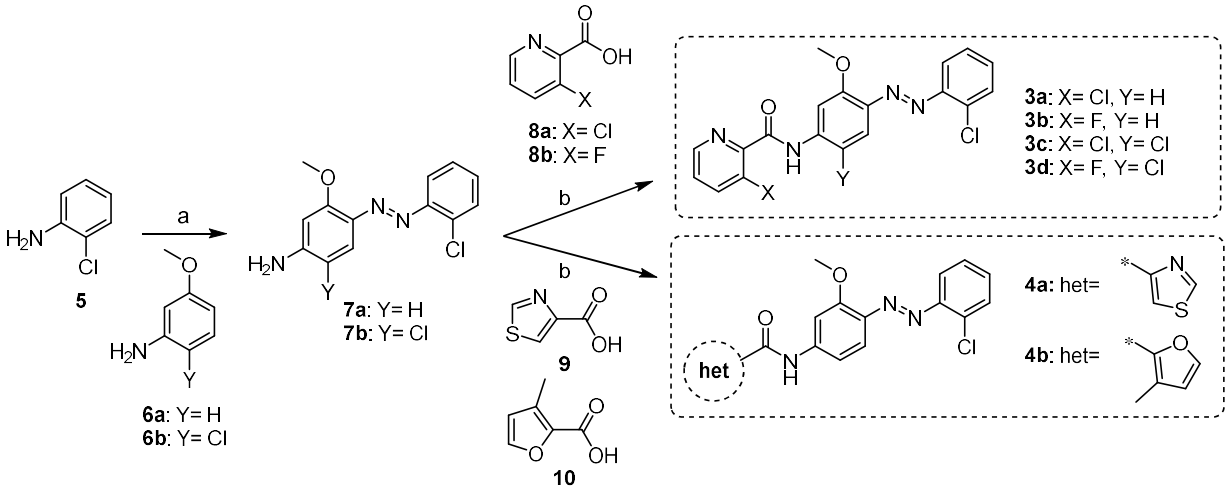

Scheme 1. Synthesis of compounds 3a-d and 4a-b. Reagents and conditions: (a) (I) conc. HCl, $NaNO_2$, 0°C, 20 min; (II) NaOAc, 0°C, 30 min, 57-85%; (b) HATU, TEA, DMF, 40-60°C, 16-48h, 21-79%.

Photochemical characterisation. The photochemical properties of **3a-d** and **4a-b** were investigated by UV/Vis absorption spectroscopy using different illumination conditions. As expected from azo compounds, samples in the dark presented the archetypical profile of *trans p-N*-amido azobenzenes including the typical *trans*-azobenzene π-π* transition band at 380-390 nm (**¡Error! No se encuentra el origen de la referencia.**, Figure 2AB, S1) (Gutzeit et al., 2021; Zussy et al., 2018). Upon illumination with different wavelengths between 365 and 560 nm, we detected a mixture with different proportions of the *cis* and the *trans* isomers in the photostationary state (PSS), which depended on the illumination wavelength. As expected, *cis* isomers showed a π-π* transition band at 270-300 nm and a weaker n−π* transition band near 430 nm, which is forbidden by the symmetry for *trans* azobenzenes. The highest proportions of *cis* isomers for all the six azo compounds were obtained upon 380 or 420-nm illumination and were back-isomerized to their thermodynamically stable *trans* isomer by using turquoise light (455-470 nm) (Figure 2AB, S1) or allowing them to thermally isomerize in the dark. The reversibility of the photoisomerization was determined by following the absorbance change upon applying several 380/455-nm alternate illumination cycles. No considerable differences were observed, showing robust photoisomerization process with no apparent degradation (Figure 2C).

Additionally, the photoisomerization of azo compound **4a** in DMSO was examined by LC-MS (Figure 2D) In the dark, 100% of *trans*-**4a** was observed, whereas a PSS of 64.5% *cis*-**4a** was detected after 385-nm illumination. Subsequent illumination with 470 nm wavelength afforded a PSS of 67.3% *trans*-**4a**. This ratio was calculated from the area of the corresponding peaks at the isosbestic point, previously determined in UV-Vis spectroscopy (*Figure 2B,C*).

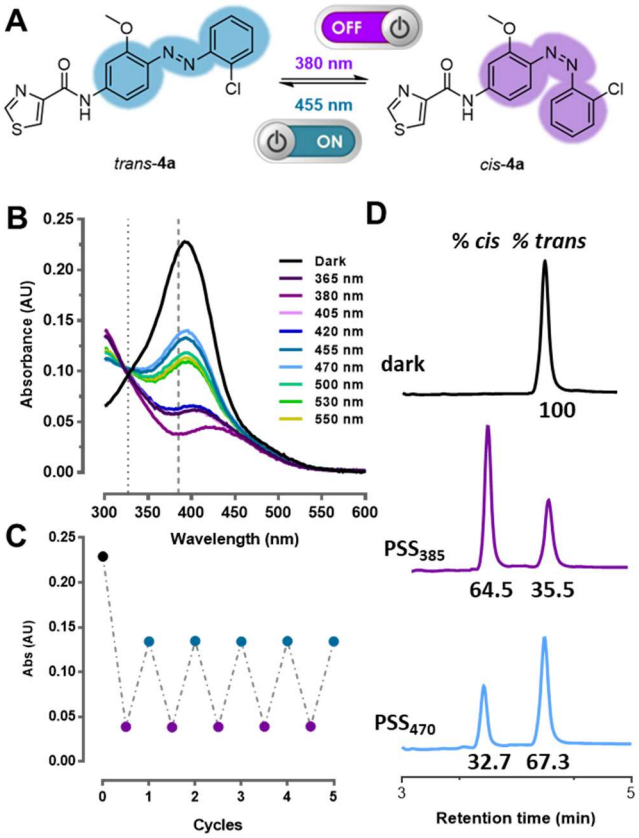

Figure 2. Photochemical properties of compound 4a. (A) Scheme of *trans/cis* isomerization; (B) UV/Vis absorption spectra of **4a** 25 µM in DMSO at 25°C under dark (black) and different light conditions for 3 min; (C) LC/MS Chromatogram of compound **4a** in the dark and at their photostationary state (PSS) after illumination with 385 or 470 nm. for 3 min with 385 and 470 nm light sources at 25°C. Samples were 100 µM in DMSO/MeCN 1:9 and chromatograms were integrated at their isosbestic point (327 nm); (D) UV/Vis absorption measurements of 50 µM **4a** in DMSO at $\lambda_{\pi\text{-}\pi^*}$max of *trans* isomer (385-390 nm) after repeated cycles of illumination with 380 (violet) and 455 nm light (turquoise).

Pharmacological characterization of 3a-d and 4a-b with IP accumulation assays. The putative $mGlu_4$ and $mGlu_6$ PAM activity of azo compounds **3a-d** and **4a-b** was determined using a cell-based inositol phosphate (IP) accumulation assay with HEK293 cells transiently expressing the corresponding mGlu receptor and a chimeric $G_{\alpha q}$ protein able to bind group II and III mGlu receptors. We first screened the compounds at single dose (30 µM) as $mGlu_4$ and $mGlu_6$ PAMs using a constant concentration of an orthosteric agonist (*i.e.* L-AP_4, 5 nM or 100 nM for $mGlu_4$ and for $mGlu_6$ receptors espectively). These measurements were done in parallel in dark and under 380 nm illumination conditions. Compounds **3c** and **3d** displayed no significant activity neither over $mGlu_4$ nor $mGlu_6$ receptor (Figure S2). Based on these data, we could confirm that the addition of a substituent in the 6-position of the central ring reduce drastically the activity in both $mGlu_4$ and $mGlu_6$ receptor. In contrast, the rest of compounds at 30 µM activated considerably $mGlu_4$ but minimally $mGlu_6$ receptor, a welcomed departure for the next experiments.

The functional activity of **3a-b** and **4a-b** was further studied through dose-response curves with the same IP accumulation assay in HEK293 cells expressing the human isoform of $mGlu_4$, $mGlu_6$ and $mGlu_8$ receptors. To evaluate the light-dependent effects, we used the same increasing concentrations of the compounds in the dark and under illumination at 380 nm in parallel. As a result, we generated concentration-response curves that allowed us to obtain the potencies (EC_{50}) for each compound under both conditions (Table 1 and Figure S3, S4 and S5). Considering the activity on $mGlu_4$ receptor, we noted that the four compounds displayed an activity in the low micromolar range in the dark, but only azo compounds **3b** and **4a** had potencies in line with Optogluram (**1**) (Table 1). In contrast, only compound **3a**, resulted practically inactive in $mGlu_6$ receptor and compound **4a** appeared to be the less active of the series in $mGlu_8$ receptor. The rest of compounds displayed a potency similar to Optogluram (**1**). When considering the assays performed under illumination, we noted that 380-nm irradiation induced a right shift of the dose-response curves as expected. This effect was compatible with a loss of the PAM potency of the *cis* isomers. This confirms that the active isomers of these new azobenzene candidates are the *trans* isomers, supporting the *trans*-on Optogluram-like approach (Table 1, Figures S3, S4 and S5). Unexpectedly, the observed photoinduced

potency shift is larger in the four azo compounds **3a-b** and **4a-b** than in Optogluram (**1**), which might induce an improved *on/off* photoswitching in more complex assays, such as *in vivo* assays.

Table 1: Photoisomerization and pharmacological properties of analogues **3a-d** and **4a-b** determined at 25 µM DMSO at 25 °C.

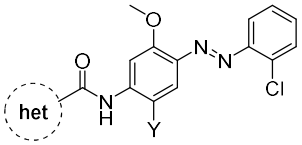

Cpd.	het	X	Y	**Photoisomerization**		**Pharmacological characterization**					
				λ_{max} (π-π^*)[a] [nm]	λ_{max} (n-π^*)[a] [nm]	$hmGlu_4$[d] pEC_{50} ± SEM		$hmGlu_6$[d] pEC_{50} ± SEM		$hmGlu_8$[d] pEC_{50} ± SEM	
				trans[b]	*PSS380*[c]	*trans*[b]	*PSS380*[c]	*trans*[b]	*PSS380*[c]	*trans*[b]	*PSS380*[c]
1		H	H	n.d.	n.d.	6.0± 0.1	5.5± 0.2	5.3± 0.0	4.7± 0.0	5.3± 0.1	4.5± 0.2
3a		Cl	H	385	434	5.2± 0.1	<4.5	<4.5	<4.5	4.5± 0.3	<4.5
3b		F	H	391	434	5.7± 0.1	4.9± 0.3	4.7± 0.2	<4.5	4.7± 0.1	<4.5
3c	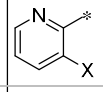	Cl	Cl	391	436	<4.5	<4.5	n.d.	n.d.	n.d.	n.d.
3d		F	Cl	390	432	<4.5	<4.5	n.d.	n.d.	n.d.	n.d.
4a		-	H	385	433	5.7± 0.1	5.2± 0.1	<4.5	<4.5	<4.5	<4.5
4b		-	H	390	435	5.3± 0.1	<4.5	<4.5	<4.5	4.7± 0.2	<4.5

[a] The absorbance maxima were extracted from UV/Vis spectra (25 µM in DMSO at 25°C). [b] Experiments performed in the dark to characterize 100% *trans* isomer.[c] Photostationary state upon Illumination with 380 nm light to obtain a high % of cis isomer. [d] The pharmacological experiments were performed with an IP accumulation assays using HEK293 cells transiently expressing the corresponding mGlu receptor subtype. Values are means of minimum 3 independent values with SEM as error bars.

Overall, compounds **3b** and **4a** displayed an activity similar to Optogluram (**1**) but only compound **4a** displays a satisfactory selectivity profile versus $mGlu_6$ and $mGlu_8$ receptors, since compound **3b** still displays considerably PAM activity on $mGlu_6$ and $mGlu_8$ receptor. Added to the improved photoswitching properties above mentioned, all these results indicate that compound **4a** emerged as the $mGlu_4$ photoswitchable PAM with the best profile to date.

Pharmacological characterization of 4a cAMP accumulation assays. We decided to further characterize the pharmacological properties of compound **4a**, named Optogluram-2. First, we wanted to confirm the results obtained in $mGlu_4$ receptor using the $G_{\alpha i/o}$ canonical pathway for the $mGlu_4$ receptor, since the IP accumulation assays used involve of a $G_{\alpha q}$ pathway, requiring a chimeric G protein. Thus, we generated concentration-response curves of **4a** using a cyclic adenosine monophosphate (cAMP) accumulation assay and using an inducible stable HEK293 cell line expressing the rat isoform of $mGlu_4$ receptor. As performed before, the light-dependent effects were evaluated in parallel, simultaneously generating two curves for each of the four azo-PAMs active, in the dark and under illumination at 380 nm. Unexpectedly, the EC_{50} obtained were in the nanomolar range ($8.4 \leq pEC_{50} \leq 6.6$, table S1, Figure 3A and S6), in contrast to the results obtained with the IP accumulation assays, which were in the low micromolar range. Nevertheless, as observed in the IP accumulation assays, compounds **3b** and **4a** had a potency in the dark more similar to Optogluram (**1**) than that of **3a** and **4b,** which were visibly less active. From

the four azo compounds, **4a** was the most potent and the one that shows a greater photoinduced potency shift (1.29 log-fold) after illuminating at 380 nm, being larger than that for Optogluram (PPS=1.00 log-fold, Table S1 and Figure 3 and S6).

To seek for the reasons of the difference of potency ranges between IP and cAMP accumulation assays and considering that we were comparing human and rat $mGlu_4$ isoforms, we also performed the IP accumulation assays with HEK293 cells transiently expressing rat $mGlu_4$ receptor (Table S1 and Figure 3 and S7). The resulting potencies for compounds **3a-b** and **4a-b** were slightly higher than those resulting from human isoform, but still in the micromolar range (ΔpEC_{50}=0.2-0.4). Therefore, the difference of potencies resulting in IP and cAMP accumulation assays cannot be associated to the human or rat isoform of $mGlu_4$ receptor, but to the intrinsic characteristics of each assay.

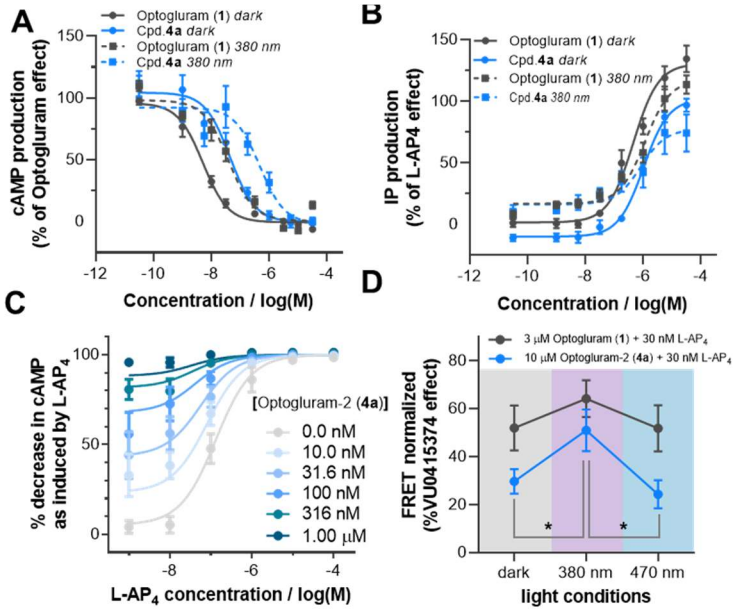

Figure 3. Pharmacological properties of Optogluram-2 (4a). Concentration-response curve of Optogluram-2 (**4a**) with a constant concentration of L-AP_4 5 nM in HEK293 stable $mGlu_4$ rat cell line with a cAMP assay (A) and in $mGlu_4$ transiently transfected rat cells with an IP assay (B) in dark conditions (rounded spots and blue solid line) and under illumination at 380 nm of wavelength (square dots and blue dotted line). Optogluram (**1**) was used as a photoswitchable $mGlu_4$ PAM standard in dark conditions (round dots and grey solid line) and under illumination at 380 nm (square dots and grey dotted line) Values are means of 4 independent values with SEM as error bars. (C) Effect of different concentrations of Optogluram-2 (**4a**) on L-AP_4 concentration-dependent activation of $mGlu_4$ receptor as determined by cAMP measurement, in dark conditions. Optogluram 2 (**4a**) modulates positively the agonistic effect of L-AP_4 and elicits intrinsic agonist activity in its *trans* configuration. Values are means of minimum 6 independent values with SEM as error bars (D). Receptor function could be efficiently controlled real-time in a reversible manner by Optogluram-2 (**4a**) through the application of 380 and 470 nm light. Values are means of 4 independent values with SEM as error bars. Analysis of variance two-way ANOVA with time as repeated measure and including the Tukey correction for multiple testing, *p < 0.05. Non-significant for Optogluram (**1**).

Allosteric interaction of Optogluram or Optogluram-2 with L-AP_4. We next studied the pharmacological profile of Optogluram-2 (**4a**) in comparison with Optogluram (**1**) by means of concentration−response curves of the agonist L-AP_4 in presence of different concentrations of the allosteric modulators using the same cAMP accumulation assay. The measurements were performed both in dark and under illumination conditions at 380 nm (

Figure **3**3C and S9). The obtained data was plotted as percentage of decrease of cAMP to account the increase of $mGlu_4$ activity prompted by the agonist and PAMs were fitted with an operational model of allosterism (Equation 1). As expected, the results confirm a positive cooperativity (i.e. increase in agonist potency) in the dark for both photoswitchable PAMs as the agonist curve is shifted to the left with increasing concentrations of the PAM. However, both azobenzene PAMs also induced an increase of basal activity, which could be associated to an allosteric agonism (i.e. ago-PAM) (Figure 3C). Upon 380-nm, both PAM effects were significantly lower. Additionally, under 380 nm light the reduction of PAM potency of Optogluram-2 (**4a**) is significantly larger than that exhibited by Optogluram (**1**) (

Figure **3**S9), confirming a more efficient $mGlu_4$ photoswitching by Optogluram-2.

Real-Time pharmacological photoswitching assays. We next evaluated the real-time photoswitching of the $mGlu_4$ activity induced by Optogluram and Optogluram-2 to confirm that that the different pharmacological effect of *cis* and *trans* isomers

can be dynamically switched with light. Thus, we used HEK293 cells expressing both $mGlu_4$ receptor and a FRET cAMP biosensor (Klarenbeek et al., 2015). First, $mGlu_4$ activity was measured after 60 minutes of cell incubation with L-AP_4 and the photoswitchable PAMs in the dark. Then, the cells were continuously illuminated with 380-nm light for 10 min to read once again the FRET and, immediately after, the cells were illuminated with 470 nm light for 10 additional minutes to finally determine the recovery of $mGlu_4$ activity. As expected, after the period in the dark, illumination with 380 nm light induced an increase of cytosolic cAMP. This was compatible with a decrease of the activity of $mGlu_4$ receptor induced by the photoisomerization of the two compounds to the less active *cis* isomer. The change in the biological response after the illumination was found to be larger for Optogluram-2 (**4a**), in agreement with IP and cAMP accumulation experiments (Figure 3D). This effect was reversed by blue illumination demonstrating a reversible photoswitching in the cellular assays as well as a dynamic control of the biological activity of $mGlu_4$ receptor with light (Figure 3D).

Selectivity profile among the mGlu subtypes. The selectivity profile of Optogluram-2 (**4a**) was also explored over the remaining mGlu subtypes at a single concentration of 30 µM with different concentrations of agonists, which was depending on the mGlu subtype and the desired effect to measure: PAM or NAM activity (Figure 4). Additionally, the selectivity of compound **4a** was compared with the selectivity of Optogluram (**1**). We used the IP accumulation assay in HEK293 cell overexpressing the corresponding receptors. Despite being slightly less potent than Optogluram (**1**) as $mGlu_4$ PAM, Optogluram-2 (**4a**) was found to selectively activate $mGlu_4$ receptor at 30 µM concentration, whereas Optogluram was also active as PAM of $mGlu_6$ and $mGlu_8$ receptors(Figure 4).

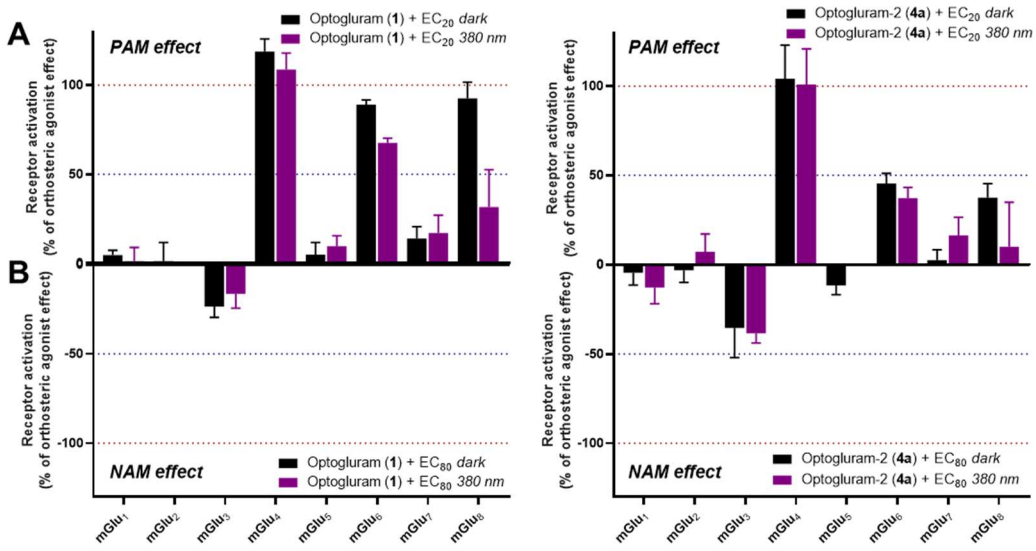

Figure 4. Selectivity profile of Optogluram (**1**, left) and Optogluram-2 (**4a**, right) among all the mGlu subtypes as PAM (A) and as NAM (B) in dark conditions (black bars) and 380 nm-illumination (violet bars).For the PAM effect evaluation, 0% corresponds to activation induced by the low dose of orthosteric agonist and 100% to the activation induced by saturating concentrations of orthosteric agonist. For the NAM effect evaluation, 0% corresponds to the activation induced by a high dose of orthosteric agonist and -100% to the basal activity with no agonist. Values are means of minimum 3 replicates with SEM as error bars.

Computational studies. To gain wider insight on the differential pharmacological properties between Optogluram (**1**) and Optogluram-2 (**4a**), we examined the molecular interactions on the allosteric pocket of both $mGlu_4$ and $mGlu_6$ receptors with a computational study to explain the differences of activity observed in the pharmacological assays and understand the $mGlu_{4/6}$ selectivity of Optogluram-2 (Figure 5AB and S10A). In our model based on the CryoEM structure of $mGlu_4$ receptor (PDB code 7E9H), VU0413574 (**2**, Figure S10, B) was positioned in a hydrophobic allosteric binding pocket inside the TM7 bundle, similar to other allosteric pockets previously described for mGlu receptors. The PAM **2** was positioned in a transversal manner allowing a strong interaction with $W798^{6.50}$ via hydrogen bond and π-π stacking and hydrogen bond with $S825^{7.36}$ (figure S10A) Despite observing a similar pose for Optogluram (**1**) and Optogluram-2 (**4a**), this last interaction was not feasible since they lack the amide bond (Figure 5AB). This may explain the higher potency of VU415374 compared to its azologues **1** and **4b**. In contrast, the models with the three ligands showed very similar hydrophobic interactions and the strong interaction with $W798^{6.50}$. Indeed, $W798^{6.50}$ is known to be crucial by mutagenesis and also believed to adopt different rotameric structures depending on the active/inactive state of the receptor (Du et al., 2021; Harpsøe et al., 2015; Pérez-Benito et al., 2017; Rovira et al., 2015). For instance, the rotameric state of the $W798^{6.50}$ in $mGlu_4$ and the closely related

$mGlu_6$ receptor differs from different crystal structures of inactive receptors such as $mGlu_1$ (PDB: 4OR2) or $mGlu_5$ (PDB: 6FFI, 7P2L) (Christopher et al., 2019; Nasrallah et al., 2021; Wu et al., 2014).

We next examined the binding mode of VU0413574 (**2**), Optogluram (**1**) and Optogluram-2 (**4a**) using a model of $mGlu_6$ transmembraane domain (TMD) based on the CryoEM structure of $mGlu_4$ receptor (PDB code 7E9H, Figure 5CD and Figure S9B) (Lin et al., 2021). Docking studies of Optogluram and Optogluram-2 (Figure 5CD) showed a similar binding mode as VU0413574 (Figure S9B). Although the binding pocket between $mGlu_4$ and $mGlu_6$ receptors is highly conserved, the binding mode of the three PAMs adopted a more vertical pose compared to the binding mode observed in $mGlu_4$. The presence of $T661^{3.40}$ in the allosteric pocket of $mGlu_6$ receptor(in contrast to $M663^{3.40}$ in $mGlu_4$ receptor) could lock the ligand in a more vertical position preventing the hydrogen bond with $W796^{6.50}$ as observed for $mGlu_4$ receptor. The resulting weaker interaction of the three compounds in the $mGlu_6$ model may result in decreased PAM potency. All three compounds presented interactions between the conserved amide moiety and $S827^{7.40}$ in the form of hydrogen bonding. Indeed, residues $S827^{7.40}$ and $T661^{3.40}$ are described to enhance the receptor activation in $mGlu_5$ receptor ($S809^{7.40}$ and $P665^{3.40}$ respectively) and, therefore, they may play an similar role in $mGlu_6$ receptor (Harpsøe et al., 2015; Lans et al., 2020; Llinas del Torrent et al., 2019). The pyridine (VU0413574 and Optogluram)/thiazole ring (Optogluram-2) were positioned in parallel to $Y665^{3.44}$ and presumably interacting by means of π-π stacking. This interaction might be the reason for the difference in potency between the two compounds, as the π-π stacking with the thiazole ring would be weaker than with the pyridine (Bootsma et al., 2019; Huber et al., 2014).

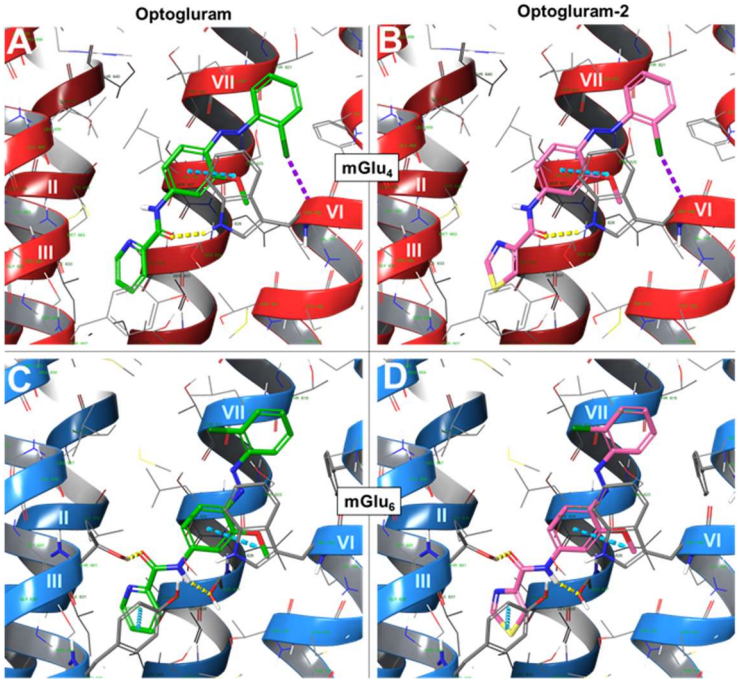

Figure 5. Computational docking of Optogluram and Optogluram-2. Binding pose of Optogluram (**1**, green, AC) and Optogluram-2 (**4a**, pink, BD) docked in the allosteric sites inside the TM7 bundle of the cryo-EM structure of $mGlu_4$ receptor (Lin et al., 2021) (AB, red, PDB 7E9H) and a homology model of $mGlu_6$ receptor (CD, blue) allosteric sites inside the TM7 bundle using Glide-XP Images made with Maestro, Schrödinger. TM5 is not shown to facilitate visual interpretation.

DISCUSSION

Photopharmacology is an emerging discipline at the interface of chemistry, biology, physics and engineering that has consolidated in the field of GPCRs to provide novel tool compounds to help the scientific community to unravel the complexity of GPCRs signalling and organization (Panarello et al., 2022). Indeed, photopharmacological tools offer the possibility to modulate the activity of a given GPCR with improved precision than conventional drugs. Use of light-sensitive ligands offers the possibility to control activity and the duration of activity at a particular location in a precise way, giving a next level of selectivity: spatiotemporal selectivity.

One of the first examples to have shown such selectivity in in a rodent preclinical model was Optogluram (**1**), reported previously by our research groups. We did not only demonstrate that we could switch on/off $mGlu_4$ activity to control the

pain sensitivity with light cycles, but also we were able to identify the signalling of amygdala $mGlu_4$ receptor as a mechanism that bypasses central sensitization processes to modulate chronic pain symptoms dynamically thanks to a photoswitchable ligand (Pereira et al., 2023; Zussy et al., 2018). However, the selectivity profile of Optogluram was not optimal, since it was also activating $mGlu_6$ receptor, and in a lower degree $mGlu_8$ receptor. Given the restricted expression of $mGlu_6$ receptor, predominantly in retina (Ferraguti et al., 2006), this lack of selectivity does not hinder the study of $mGlu_4$ biological function in different brain areas. However, for the study of $mGlu_6$ receptor in the eye, this paradigm can be different, as there are evidences both $mGlu_6$ and $mGlu_4$ receptors are expressed (Guimarães-Souza et al., 2012; Quraishi et al., 2007; Zhang et al., 2020). In this case, the availability of photoswitchable compounds either selective for $mGlu_4$ or $mGlu_6$ receptors are required to distinguish the effects associated to a single receptor subtype.

In the present work, we synthesized a small library of photo switchable analogues of Optogluram changing the substitution of the central or pyridine ring with the aim of conserving $mGlu_4$ activity and hopefully losing $mGlu_6$ activity. We found that azocompound **4a** (Optogluram-2) acted as a PAM of $mGlu_4$ receptor using an IP accumulation assay with a chimeric G_q protein. In such assay, Optogluram-2 had slightly reduced potency than Optogluram but had an improved selectivity over other mGlu receptors, including $mGlu_6$ and $mGlu_8$ receptors.

We further analysed the pharmacological properties of Optogluram and Optogluram-2 using rat $mGlu_4$ receptor with the same IP accumulation assay and also using a cAMP accumulation assay, that monitors the canonical signalling pathway. In all cases, Optogluram-2 had a similar or an improved photoswitching upon 380-nm illumination compared to its reference azocompound (Optogluram). These properties were additionally confirmed by real-time photoswitching of $mGlu_4$ activity. We observed a decrease of the $mGlu_4$ activation for both Optogluram and Optogluram-2 upon illumination with violet light (380 nm) and a PAM activity recovery after blue light (470 nm) exposition. However, the photoswitching observed for Optogluram-2 had a higher degree of statistical significance, involving and improved photoregulation of $mGlu_4$ activity.

We also studied the type of allosteric modulation of Optogluram and Optogluram-2 by means of functional interactions with L-AP_4, and data were fitted to an operational model of allosterism. These data suggested that both PAMs have a positive cooperativity with the orthosteric agonist and can potentiate its effect but, importantly, they also show allosteric agonism (i.e. they are agoPAMs). Though, this might also be a result of potentiation of the agonistic effect of the residual endogenous glutamate that the cells naturally produce. However this last option is not likely as the original compound, VU0415374 (**2**), has been reported to be agoPAM with a very similar allosteric profile (Rovira et al., 2015). Computational modelling shown here suggest that VU0415374, Optogluram and Optogluram-2 share the same binding mode in the allosteric pocket inside the transmembrane domain of $mGlu_4$ receptor. Very recently, during our manuscript writing step, a new different binding mode has been reported in a novel $mGlu_4$ cryoEM structure for the structurally related PAM VU0364770. In such structure, the shorter bicyclic VU0364770 is bound in the interprotomer interface between TM1,6,7 and TM6 from each subunit respectively (Wang et al., 2023). In contrast, we proposed a binding site for PAMs **1**, **2** and **4a** in the active subunit between helixes TM2,3,6,7, which is in very good agreement with previous mutagenesis studies in $mGlu_4$ receptor with VU0415374 (**2**) and other similar PAMs (Rovira et al., 2015). We hypothesise that both binding pockets may exist in $mGlu_4$ homodimer, where either two PAM ligand units may bind or one pocket may be a vestibule for the second one. However, proving this hypothesis would need several experiments and it is out of the scope of the present study. The binding site of the three compounds in an $mGlu_6$ receptor homology model was located in the same region of the TMD, however, the binding mode was slightly different. In this last case, it was characterised to have less strong but more numerous interactions. Between them, it is important to point out a π-π stacking between $Tyr665^{3.44}$ and the ligand heterocyclic ring. Indeed π-π stacking energies may be very different depending on the nature of the heterocycles(Bootsma et al., 2019; Huber et al., 2014) and there are high chances that this is the reason behind the difference of activity between Optogluram and Optogluram-2 in $mGlu_6$ receptor.

Despite Optogluram-2 has a slightly reduced potency in $mGlu_4$ receptor compared to Optogluram, its enhanced photoswitching behaviour and improved selectivity makes it an excellent candidate to study the roles of $mGlu_4$ receptor with an improved spatiotemporal precision. Indeed, the use of Optogluram can lead to imprecise conclusions if the doses of the compound and light are not very well adjusted in tissues such as retina that can express both $mGlu_4$ and $mGlu_6$ receptors (Guimarães-Souza et al., 2012; Quraishi et al., 2007; Zhang et al., 2020) or in several areas of the CNS where $mGlu_4$ and $mGlu_8$ receptors are co-expressed (Ferraguti et al., 2006), especially if Optogluram is administered via systemic injections. Optogluram-2 may not share these difficulties. Overall, Optogluram-2 showed improved photoswitching properties and selectivity profile than Optogluram, which is one of the photopharmacological tools better advanced and more successful in

vivo to date (Pereira et al., 2023; Zussy et al., 2018). All this makes Optogluram-2 an important reference tool compound to study the role of $mGlu_4$ receptor in pathophysiological networks with high spatiotemporal precision.

ASSOCIATED CONTENT

Supporting Information includes supporting figures, synthetic procedures, NMR spectra, HPLC-PDA-MS data and HRMS data.

AUTHOR INFORMATION

Corresponding Authors

* MCS, Institute for Advanced Chemistry of Catalonia
Spanish National Research Council (CSIC)
Jordi Girona 18-16, 08034 Barcelona, Spain
amadeu.llebaria@iqac.csic.es
xavier.gomez@iqac.csic.es

Present Addresses

†Enantia, Barcelona, Spain

‡Exscientia, Oxford OX4 4GE, United Kingdom.

Author Contributions

The manuscript was written through contributions of all authors and all have given approval to the final version of the manuscript.

ACKNOWLEDGMENTS

We thank Carme Serra and Lourdes Muñoz from SIMChem (IQAC CSIC) for the use of analytical support and helpful discussions. ARPEGE Pharmacology-Screening-Interactome platform facility (UMS Bio-campus, Montpellier, France) for the use the plate readers. REVVITY (former PerkinElmer-Cisbio) for providing HTRF cAMP and IPOne kits in the frame of EIDOS collaborative laboratory. H. Gutierrez-de-Teran for computational support. The results included in this standard have received funding from the European Union's Horizon 2020 research and innovation programme under Marie Skłodowska-Curie grant agreement No. 801342 (Tecniospring INDUSTRY, TECSPR19-1-0062) and the Government of Catalonia's Agency for Business Competitiveness (ACCIÓ) to XGS, Agence Nationale de la Recherche (ANR-17-CE11-0046) to JPP, Labex EpiGenMed (ANR-10-LABX-12-01) to JPP, Fondation Recherche Médicale (FRM DEQ20170336747) to JPP, from the NEURON Research Programme which is jointly funded by national funding authorities within the framework of the ERA-NET NEURON (ANR-17-NEU3–0001) to CG and AL, the CNRS International Scientific Collaboration Program (PICS 08212) to CG, AL and XR, Ministerio de Ciencia e Innovación, Agencia Estatal de Investigación and ERDF - A way of making Europe (CTQ2017-89222-R, PCI2018-093047, PID2020-120499RB-I00, PIE-RYC2020--029485-I) to AL and XR, by the Catalan government (2021 SGR 00508) to AL and by the Spanish National Research Council (20228AT014) to XR. We thank the European Research Network on Signal Transduction (ERNEST Cost Action 18133) and the International Research Network on GPCRs (iGPCRnet) to finance the diffusion of our research.

CONFLICT OF INTEREST

The authors declare no conflict of interest

REFERENCES

Bootsma, A. N., Doney, A. C., & Wheeler, S. E. (2019). Predicting the Strength of Stacking Interactions between Heterocycles and Aromatic Amino Acid Side Chains. *Journal of the American Chemical Society*, *141*(28), 11027–11035. doi: 10.1021/jacs.9b00936

Bossi, S., Helleringer, R., Galante, M., Monlleó, E., Trapero, A., Rovira, X., Daniel, H., Llebaria, A., & McLean, H. (2018). A light-controlled allosteric modulator unveils a role for mGlu4 receptors during early stages of ischemia in the rodent cerebellar cortex. *Frontiers in Cellular Neuroscience*, *12*(November), 1–15. doi: 10.3389/fncel.2018.00449

Calabrese, V., Picconi, B., Heck, N., Campanelli, F., Natale, G., Marino, G., Sciaccaluga, M., Ghiglieri, V., Tozzi, A., Anceaume,

E., Cuoc, E., Caboche, J., Conquet, F., Calabresi, P., & Charvin, D. (2022). A positive allosteric modulator of mGlu4 receptors restores striatal plasticity in an animal model of l-Dopa-induced dyskinesia. *Neuropharmacology*, *218*, 109205. doi: 10.1016/J.NEUROPHARM.2022.109205

Celli, R., Santolini, I., Luijtelaar, G. Van, Ngomba, R. T., Nicoletti, F., Celli, R., Santolini, I., Luijtelaar, G. Van, & Ngomba, R. T. (2019). Targeting metabotropic glutamate receptors in the treatment of epilepsy: rationale and current status. *Expert Opinion on Therapeutic Targets*, *23*(4), 341–351. doi: 10.1080/14728222.2019.1586885

Christopher, J. A., Orgován, Z., Congreve, M., Doré, A. S., Errey, J. C., Marshall, F. H., Mason, J. S., Okrasa, K., Rucktooa, P., Serrano-Vega, M. J., Ferenczy, G. G., & Keseru, G. M. (2019). Structure-Based Optimization Strategies for G Protein-Coupled Receptor (GPCR) Allosteric Modulators: A Case Study from Analyses of New Metabotropic Glutamate Receptor 5 (mGlu 5) X-ray Structures. *Journal of Medicinal Chemistry*, *62*(1), 207–222. doi: 10.1021/acs.jmedchem.7b01722

Davis, M. J., Iancu, O. D., Acher, F. C., Stewart, B. M., Eiwaz, M. A., Duvoisin, R. M., & Raber, J. (2013). Role of mGluR4 in acquisition of fear learning and memory. *Neuropharmacology*, *66*, 365–372. doi: 10.1016/j.neuropharm.2012.07.038

Donthamsetti, P., Konrad, D. B., Hetzler, B., Fu, Z., Trauner, D., & Isacoff, E. Y. (2021). Selective Photoswitchable Allosteric Agonist of a G Protein-Coupled Receptor. *Journal of the American Chemical Society*, *143*(24), 8951–8956. doi: 10.1021/jacs.1c02586

Du, J., Wang, D., Fan, H., Xu, C., Tai, L., Lin, S., Han, S., Tan, Q., Wang, X., Xu, T., Zhang, H., Chu, X., Yi, C., Liu, P., Wang, X., Zhou, Y., Pin, J. P., Rondard, P., Liu, H., … Zhao, Q. (2021). Structures of human mGlu2 and mGlu7 homo- and heterodimers. *Nature 2021 594:7864*, *594*(7864), 589–593. doi: 10.1038/s41586-021-03641-w

Engers, D. W., Field, J. R., Le, U., Zhou, Y., Bolinger, J. D., Zamorano, R., Blobaum, A. L., Jones, C. K., Jadhav, S., Weaver, C. D., Conn, P. J., Lindsley, C. W., Niswender, C. M., & Hopkins, C. R. (2011). Discovery, synthesis, and structure-activity relationship development of a series of N-(4-acetamido)phenylpicolinamides as positive allosteric modulators of metabotropic glutamate receptor 4 (mGlu(4)) with CNS exposure in rats. *Journal of Medicinal Chemistry*, *54*(4), 1106–1110. doi: 10.1021/jm101271s

Ferraguti, F., & Shigemoto, R. (2006). Metabotropic glutamate receptors. *Cell and Tissue Research*, *326*(2), 483–504. doi: 10.1007/s00441-006-0266-5

Fredriksson, R., Lagerström, M. C., Lundin, L. G., & Schiöth, H. B. (2003). The G-protein-coupled receptors in the human genome form five main families. Phylogenetic analysis, paralogon groups, and fingerprints. *Molecular Pharmacology*, *63*(6), 1256–1272. doi: 10.1124/mol.63.6.1256

Girard, B., Tuduri, P., Moreno, M. P., Sakkaki, S., Barboux, C., Bouschet, T., Varrault, A., Vitre, J., McCort-Tranchepain, I., Dairou, J., Acher, F., Fagni, L., Marchi, N., Perroy, J., & Bertaso, F. (2019). The mGlu7 receptor provides protective effects against epileptogenesis and epileptic seizures. *Neurobiology of Disease*, *129*, 13–28. doi: 10.1016/J.NBD.2019.04.016

Gómez-Santacana, X., Panarello, S., & Rovira, X. (2022). Pharmacology Photoswitchable allosteric modulators for metabotropic glutamate receptors. *Current Opinion in Pharmacology*, *66*, 102266. doi: 10.1016/j.coph.2022.102266

Gómez-Santacana, X., Pittolo, S., Rovira, X., Lopez, M., Zussy, C., Dalton, J. A. R., Faucherre, A., Jopling, C., Pin, J. P., Ciruela, F., Goudet, C., Giraldo, J., Gorostiza, P., & Llebaria, A. (2017). Illuminating Phenylazopyridines to Photoswitch Metabotropic Glutamate Receptors: From the Flask to the Animals. *ACS Central Science*, *3*(1), 81–91. doi: 10.1021/acscentsci.6b00353

Gradini, R., Ngomba, R., Nicoletti, F., Bruno, V., Ngomba, R. T., Gradini, R., & Battaglia, G. (2015). Metabotropic glutamate receptors as drug targets: what's new? *Current Opinion in Pharmacology*, *20*, 89–94. doi: 10.1016/j.coph.2014.12.002

Gregory, K. J., & Goudet, C. (2021). International Union of Basic and Clinical Pharmacology. CXI. Pharmacology, Signaling, and Physiology of Metabotropic Glutamate Receptors. *Pharmacological Reviews*, *73*(1), 521–569. doi: 10.1124/PR.119.019133

Guimarães-Souza, E. M., & Calaza, K. C. (2012). Selective activation of group III metabotropic glutamate receptor subtypes produces different patterns of γ-aminobutyric acid immunoreactivity and glutamate release in the retina. *Journal of Neuroscience Research*, *90*(12), 2349–2361. doi: 10.1002/JNR.23123

Gutzeit, V. A., Acosta-Ruiz, A., Munguba, H., Häfner, S., Landra-Willm, A., Mathes, B., Mony, J., Yarotski, D., Börjesson, K., Liston, C., Sandoz, G., Levitz, J., & Broichhagen, J. (2021). A fine-tuned azobenzene for enhanced photopharmacology in vivo. *Cell Chemical Biology*, *28*, 1–16. doi: 10.1016/j.chembiol.2021.02.020

Harpsøe, K., Isberg, V., Tehan, B. G., Weiss, D., Arsova, A., Marshall, F. H., Bräuner-Osborne, H., & Gloriam, D. E. (2015).

Selective Negative Allosteric Modulation Of Metabotropic Glutamate Receptors – A Structural Perspective of Ligands and Mutants. *Scientific Reports 2015 5:1*, *5*(1), 1–11. doi: 10.1038/srep13869

Huber, R. G., Margreiter, M. A., Fuchs, J. E., Von Grafenstein, S., Tautermann, C. S., Liedl, K. R., & Fox, T. (2014). Heteroaromatic π-stacking energy landscapes. *Journal of Chemical Information and Modeling*, *54*(5), 1371–1379. doi: 10.1021/ci500183u

Hüll, K., Morstein, J., & Trauner, D. (2018). In Vivo Photopharmacology. *Chemical Reviews*, *118*(21), 10710–10747. doi: 10.1021/acs.chemrev.8b00037

Klarenbeek, J., Goedhart, J., Van Batenburg, A., Groenewald, D., & Jalink, K. (2015). Fourth-Generation Epac-Based FRET Sensors for cAMP Feature Exceptional Brightness, Photostability and Dynamic Range: Characterization of Dedicated Sensors for FLIM, for Ratiometry and with High Affinity. *PLOS ONE*, *10*(4), e0122513. doi: 10.1371/JOURNAL.PONE.0122513

Lans, I., Díaz, Ó., Dalton, J. A. R., & Giraldo, J. (2020). Exploring the Activation Mechanism of the mGlu5 Transmembrane Domain. *Frontiers in Molecular Biosciences*, *7*, 513462. doi: 10.3389/FMOLB.2020.00038/BIBTEX

Lin, S., Han, S., Cai, X., Tan, Q., Zhou, K., Wang, D., Wang, X., Du, J., Yi, C., Chu, X., Dai, A., Zhou, Y., Chen, Y., Zhou, Y., Liu, H., Liu, J., Yang, D., Wang, M. W., Zhao, Q., & Wu, B. (2021). Structures of Gi-bound metabotropic glutamate receptors mGlu2 and mGlu4. *Nature 2021 594:7864*, *594*(7864), 583–588. doi: 10.1038/s41586-021-03495-2

Lindsley, C. W., Emmitte, K. A., Hopkins, C. R., Bridges, T. M., Gregory, K. J., Niswender, C. M., & Conn, P. J. (2016). Practical Strategies and Concepts in GPCR Allosteric Modulator Discovery: Recent Advances with Metabotropic Glutamate Receptors. *Chemical Reviews*, *116*(11), 6707–6741. doi: 10.1021/acs.chemrev.5b00656

Llinas del Torrent, C., Pérez-Benito, L., & Tresadern, G. (2019). Computational Drug Design Applied to the Study of Metabotropic Glutamate Receptors. *Molecules*, *24*(1098), 1–22. doi: 10.3390/molecules24061098

Luessen, D. J., & Conn, P. J. (2022). Allosteric Modulators of Metabotropic Glutamate Receptors as Novel Therapeutics for Neuropsychiatric Disease. *Pharmacological Reviews*, *74*(3), 630–661. doi: 10.1124/PHARMREV.121.000540

Marino, M. J., Hess, J. F., & Liverton, N. (2005). Targeting the Metabotropic Glutamate Receptor mGluR4 for the Treatment of Diseases of the Central Nervous System. *Current Topics in Medicinal Chemistry*, *5*, 885–895. doi: 10.2174/1568026054750263

Nasrallah, C., Cannone, G., Briot, J., Rottier, K., Berizzi, A. E., Huang, C. Y., Quast, R. B., Hoh, F., Banères, J. L., Malhaire, F., Berto, L., Dumazer, A., Font-Ingles, J., Gómez-Santacana, X., Catena, J., Kniazeff, J., Goudet, C., Llebaria, A., Pin, J. P., … Lebon, G. (2021). Agonists and allosteric modulators promote signaling from different metabotropic glutamate receptor 5 conformations. *Cell Reports*, *36*(9), 109648. doi: 10.1016/J.CELREP.2021.109648

Nickols, H. H., & Conn, J. P. (2014). Development of allosteric modulators of GPCRs for treatment of CNS disorders. *Neurobiology of Disease*, *61*, 55–71. doi: 10.1016/j.nbd.2013.09.013

Panarello, S., Rovira, X., Llebaria, A., & Gómez-Santacana, X. (2022). Photopharmacology of G-Protein-Coupled Receptors. In Zbigniew L. Pianowski (Ed.), Molecular Photoswitches: Synthesis, Properties and Applications. (pp. 921–944). John Wiley & Sons, Ltd. doi: 10.1002/9783527827626.CH37

Panarese, J. D., Engers, D. W., Wu, Y. J., Bronson, J. J., Macor, J. E., Chun, A., Rodriguez, A. L., Felts, A. S., Engers, J. L., Loch, M. T., Emmitte, K. A., Castelhano, A. L., Kates, M. J., Nader, M. A., Jones, C. K., Blobaum, A. L., Conn, P. J., Niswender, C. M., Hopkins, C. R., & Lindsley, C. W. (2019). Discovery of VU2957 (Valiglurax): An mGlu 4 Positive Allosteric Modulator Evaluated as a Preclinical Candidate for the Treatment of Parkinson's Disease. *ACS Medicinal Chemistry Letters*, *10*(3), 255–260. doi: 10.1021/acsmedchemlett.8b00426

Pereira, V., Arias, J. A., Llebaria, A., & Goudet, C. (2023). Photopharmacological manipulation of amygdala metabotropic glutamate receptor mGlu4 alleviates neuropathic pain. *Pharmacological Research*, *187*, 106602. doi: 10.1016/J.PHRS.2022.106602

Pereira, V., & Goudet, C. (2019). Emerging trends in pain modulation by metabotropic glutamate receptors. *Frontiers in Molecular Neuroscience*, *11*, 424363. doi: 10.3389/FNMOL.2018.00464/BIBTEX

Pérez-Benito, L., Doornbos, M. L. J., Cordomí, A., Peeters, L., Lavreysen, H., Pardo, L., & Tresadern, G. (2017). Molecular Switches of Allosteric Modulation of the Metabotropic Glutamate 2 Receptor. *Structure*, *25*(7), 1153-1162.e4. doi: 10.1016/J.STR.2017.05.021

Pittolo, S., Gómez-Santacana, X., Eckelt, K., Rovira, X., Dalton, J., Goudet, C., Pin, J. P., Llobet, A., Giraldo, J., Llebaria, A., &

Gorostiza, P. (2014). An allosteric modulator to control endogenous G protein-coupled receptors with light. *Nature Chemical Biology*, *10*(10), 813–815. doi: 10.1038/nchembio.1612

Pittolo, S., Lee, H., Lladó, A., Tosi, S., Bosch, M., Bardia, L., Gómez-Santacana, X., Llebaria, A., Soriano, E., Colombelli, J., Poskanzer, K. E., Perea, G., & Gorostiza, P. (2019). Reversible silencing of endogenous receptors in intact brain tissue using 2-photon pharmacology. *Proceedings of the National Academy of Sciences of the United States of America*, *116*(27). doi: 10.1073/pnas.1900430116

Quraishi, S., Gayet, J., Morgans, C. W., & Duvoisin, R. M. (2007). Distribution of group-III metabotropic glutamate receptors in the retina. *Journal of Comparative Neurology*, *501*(6), 931–943. doi: 10.1002/CNE.21274

Raber, J., & Duvoisin, R. M. (2015). Novel metabotropic glutamate receptor 4 and glutamate receptor 8 therapeutics for the treatment of anxiety. *Expert Opinion on Investigational Drugs*, *24*(4), 519–528. doi: 10.1517/13543784.2014.986264

Rascol, O., Medori, R., Baayen, C., Such, P., & Meulien, D. (2022). A Randomized, Double-Blind, Controlled Phase II Study of Foliglurax in Parkinson's Disease. *Movement Disorders*, *37*(5), 1088–1093. doi: 10.1002/MDS.28970

Ricart-Ortega, M., Berizzi, A. E., Pereira, V., Malhaire, F., Catena, J., Font, J., Gómez-Santacana, X., Munõz, L., Zussy, C., Serra, C., Rovira, X., Goudet, C., & Llebaria, A. (2020). Mechanistic Insights into Light-Driven Allosteric Control of GPCR Biological Activity. *ACS Pharmacology and Translational Science*, *3*(5), 883–895. doi: 10.1021/acsptsci.0c00054

Ricart-Ortega, M., Font, J., & Llebaria, A. (2019). GPCR photopharmacology. In Molecular and Cellular Endocrinology (Vol. 488, pp. 36–51). Elsevier. doi: 10.1016/j.mce.2019.03.003

Rovira, X., Malhaire, F., Scholler, P., Rodrigo, J., Gonzalez-Bulnes, P., Llebaria, A., Pin, J. P., Giraldo, J., & Goudet, C. (2015). Overlapping binding sites drive allosteric agonism and positive cooperativity in type 4 metabotropic glutamate receptors. *The FASEB Journal*, *29*(1), 116–130. doi: 10.1096/FJ.14-257287

Rovira, X., Trapero, A., Pittolo, S., Zussy, C., Faucherre, A., Jopling, C., Giraldo, J., Pin, J. P., Gorostiza, P., Goudet, C., & Llebaria, A. (2016). OptoGluNAM4.1, a Photoswitchable Allosteric Antagonist for Real-Time Control of mGlu4 Receptor Activity. *Cell Chemical Biology*, *23*(8), 929–934. doi: 10.1016/j.chembiol.2016.06.013

Schiöth, H. B., & Lagerström, M. C. (2008). Structural diversity of g proteincoupled receptors and significance for drug discovery. *Nature Reviews Drug Discovery*, *7*(4), 339–357. doi: 10.1038/nrd2518

Sheffler, D. J., Gregory, K. J., Rook, J. M., & Conn, P. J. (2011). Allosteric Modulation of Metabotropic Glutamate Receptors. In Advances in Pharmacology (1st ed., Vol. 62, pp. 37–77). Elsevier Inc. doi: 10.1016/B978-0-12-385952-5.00010-5

Sriram, K., & Insel, P. A. (2018). GPCRs as targets for approved drugs: How many targets and how many drugs? *Molecular Pharmacology*, *93*(4), 251–258. doi: 10.1124/MOL.117.111062

Stansley, B. J., & Conn, P. J. (2019). Neuropharmacological Insight from Allosteric Modulation of mGlu Receptors. *Trends in Pharmacological Sciences*, *40*(4), 240–252. doi: 10.1016/J.TIPS.2019.02.006

Szymański, W., Beierle, J. M., Kistemaker, H. A. V., Velema, W. A., & Feringa, B. L. (2013). Reversible photocontrol of biological systems by the incorporation of molecular photoswitches. *Chemical Reviews*, *113*(8), 6114–6178. doi: 10.1021/cr300179f

Wang, X., Wang, M., Xu, T., Feng, Y., Shao, Q., Han, S., Chu, X., Xu, Y., Lin, S., Zhao, Q., & Wu, B. (2023). Structural insights into dimerization and activation of the mGlu2–mGlu3 and mGlu2–mGlu4 heterodimers. *Cell Research 2023*, 1–13. doi: 10.1038/s41422-023-00830-2

Witkin, J. M., Pandey, K. P., & Smith, J. L. (2022). Clinical investigations of compounds targeting metabotropic glutamate receptors. *Pharmacology Biochemistry and Behavior*, *219*, 173446. doi: 10.1016/J.PBB.2022.173446

Wu, H., Wang, C., Gregory, K. J., Han, G. W., Cho, H. P., Xia, Y., Niswender, C. M., Katritch, V., Meiler, J., Cherezov, V., Conn, P. J., & Stevens, R. C. (2014). Structure of a class C GPCR metabotropic glutamate receptor 1 bound to an allosteric modulator. *Science*, *344*(6179), 58–64. doi: 10.1126/science.1249489

Zhang, Z., Liu, Y., Luan, Y., Zhu, K., Hu, B., Ma, B., Chen, L., Liu, X., Lu, H., Chen, X., Liu, Y., & Zheng, X. (2020). Activation of Type 4 Metabotropic Glutamate Receptor Regulates Proliferation and Neuronal Differentiation in a Cultured Rat Retinal Progenitor Cell Through the Suppression of the cAMP/PTEN/AKT Pathway. *Frontiers in Molecular Neuroscience*, *13*, 534310. doi: 10.3389/FNMOL.2020.00141/BIBTEX

Zussy, C., Gómez-Santacana, X., Rovira, X., De Bundel, D., Ferrazzo, S., Bosch, D., Asede, D., Malhaire, F., Acher, F., Giraldo, J., Valjent, E., Ehrlich, I., Ferraguti, F., Pin, J.-P. P., Llebaria, A., & Goudet, C. (2018). Dynamic modulation of inflammatory

pain-related affective and sensory symptoms by optical control of amygdala metabotropic glutamate receptor 4. *Molecular Psychiatry*, *23*(3), 509–520. doi: 10.1038/mp.2016.223